

**SMASIS2018-8049**

## **DESIGN OF A VARIABLE STIFFNESS WRIST BRACE WITH AN ORIGAMI STRUCTURAL ELEMENT**

**Marcos B. Oliveira**

Expeditionary Robotics Lab  
Mechanical and Industrial Engineering  
Northeastern University  
Boston, Massachusetts 02115  
Email: oliveira.ma@husky.neu.edu

**Chang Liu**

Expeditionary Robotics Lab  
Mechanical and Industrial Engineering  
Northeastern University  
Boston, Massachusetts 02115  
Email: liu.chang7@husky.neu.edu

**Mengtao Zhao**

Expeditionary Robotics Lab  
Mechanical and Industrial Engineering  
Northeastern University  
Boston, Massachusetts 02115  
Email: zhao.meng@husky.neu.edu

**Samuel M. Felton\***

Expeditionary Robotics Lab  
Mechanical and Industrial Engineering  
Northeastern University  
Boston, Massachusetts 02115  
Email: s.felton@northeastern.edu

### **ABSTRACT**

*This paper presents a motor driven wrist brace that can adjust its stiffness by changing its mesoscale geometry. The design involves a plate structure that folds from a flexible flat shape to a stiff corrugated shape by means of a motor driven tendon. The structure is built using a laminate of rigid and flexible layers, with embedded flexural hinges that allow it to fold. The paper proposes a simplified analytical model to predict stiffness, and physical three-point bending tests indicate that the brace can increase its stiffness up to fifty times by folding.*

### **INTRODUCTION**

The design of wearable devices requires a compromise between flexibility and rigidity. The former requirement is usually associated with comfort and noninvasiveness while the latter is closely related to injury prevention and precision. To better balance these competing goals, some devices actively adjust their stiffness. These include pneumatic operated splints [1] [2], motor

driven exosuits [3], and orthopedic casts [4]. Designs must balance criteria such as stiffness ratio, ultimate (or yield) stress, activation time, scalability, medical requirements, operational spectrum (binary or continuous), reversibility [5] and comfort.

A classification based on the working principles of proposed solutions found in the literature for stiffness variability is presented in [5]. Each solution is based on at least one of three main perspectives: mechanical, material and/or geometrical. For mechanical based approaches, the system adjusts its own stiffness by changing the boundary conditions to which it is subjected. For instance, Jafari et al [6] presented an actuator with adjustable stiffness (AwAS) based on the variation of a lever arm by perpendicular positioning of spring elements and the pivot point.

For a material based approach, one adjusts the elastic properties of a structure by either altering its elastic material properties and/or the internal interactions between its structural components. Proposed methods involving a direct change in the elastic material properties include phase transition [7], glass transition (shape memory material) [8], rheological fluids (electro- and magneto-rheological fluids) [9, 10], and granular and multi-layer

---

\*Address all correspondence to this author.



**FIGURE 1:** Wrist brace design based on a self-folding hinged structure.

jamming [2, 11–13].

The third approach involves tuning of geometrical properties. Changes to the cross-section configuration (shape and/or dimensions) influence the second moment of area altering the ultimate bending stiffness of a structure. By reconfiguring the cross-sectional geometry in such a way that the amount of material distal to the neutral axis is maximized, one can obtain significant changes in the second moment of area about this axis which affects the ultimate structural stiffness [5]. In this category, a vast range of solutions are proposed based on self-folding devices [14] and reconfigurable structures [15]. Based on the high load bearing to weight ratio [16] and a compact form usually associated with these methods we propose a self-folding motor driven wrist brace. Change in stiffness is obtained by switching between a low inertial state (which we call “flat”) and a high inertial state (hereafter called “corrugated”).

The device presented aims at assisting people who suffer from carpal tunnel syndrome. Individuals diagnosed with carpal tunnel syndrome are usually treated with splints or braces that keep the user’s wrist in a neutral position preventing any movements that would cause pain and discomfort [17]. These devices are usually applied at night when an individual cannot consciously control his/her wrist orientation while asleep. However, they may cause discomfort or hinder movement when the wrist is already in a neutral position or when one needs to perform tasks involving quick (and benign) bending of his/her hand. Considering the easy fabrication procedures associated with the proposed wrist brace and the stiffness ratios that can be obtained, our design proves to be a promising approach to orthopedic devices requiring control over stiffness (Fig. 1). The wrist brace introduced in this paper represents a proof-of-concept that an origami-based variable-stiffness brace can selectively immobilize the wrist.

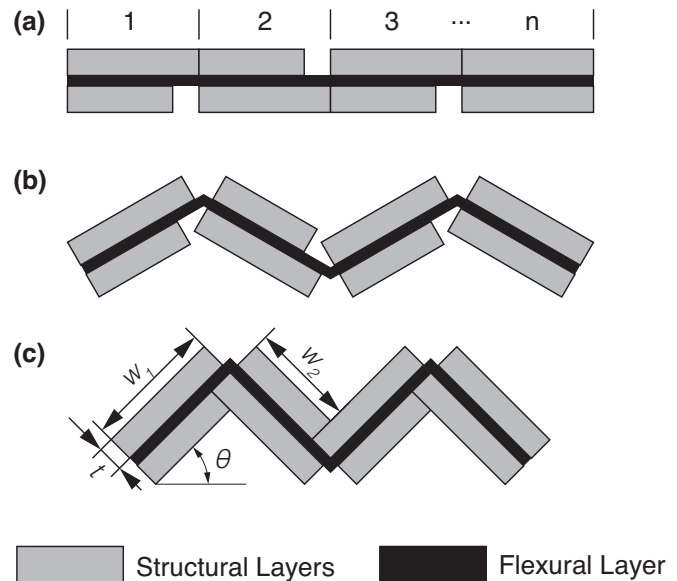


**FIGURE 2:** Corrugated shape design with eight individual beams. (a) Flat Mode. (b) Intermediate mode. (c) Final corrugated design.

## DESIGN AND FABRICATION

### Corrugated Shape Design

The wrist brace consists of a composite hinged structure attached to a spongy glove with a microprocessor board attached to it. The hinged structure is a three-layer sandwiched laminate (Fig. 2). A flexural layer using 50  $\mu\text{m}$  thick nylon film is bonded to two outer rigid layers. Gaps are cut in the rigid layers to allow the flexural layer to bend freely, creating flexural hinges. These gaps are offset so that the rigid layers interlock when folded.

The structure transforms from a flat mode (Fig. 2a), passing through intermediate corrugated modes (Fig. 2.b) to a final desired corrugated shape characterized by angle  $\theta$  (Fig. 2c) by bending at these hinges. A tendon connecting adjacent multi-layered tabs drives the folding process. Control over the final corrugated angle is obtained by leaving alternated gaps on the top and bottom faces of the hinged structure [18] between adjacent tabs.

### Fabrication

The fabrication method for the hinged structure used a laminate approach optimized in previous research [19]. To properly locate the stacking of multiple layers, we laser cut both the bottom and top layers of rigid material with four alignment holes distributed on the sides of these plates. We then sandwich the flexural layer of nylon film with both top and bottom layers of rigid material by using adhesive transfer tape and alignment

dowel pins. In order to separate the tabs and obtain the hinged structure, a release cut is performed on the extremities of the laminate for the specific final length desired using a laser cutter. In order to decrease frictional forces on the holes where the actuating tendon is present, we chamfered the holes using hand-held deburring tools. Additional control over the angle of corrugation is provided by threading the tendon inside acrylic “stoppers” placed on the internal side of folds (Fig. 3).

A small 6V gear motor (Pololu 298:1 HPCB 6V) was mounted with a 3D printed motor bracket custom designed for this specific application. The bracket was fixed to the hinged structure with a pair of M3 nuts and bolts on each side of the bracket. This arrangement allowed for a low profile design of the wrist brace.

Based on previous work [3], the material used on this component was neoprene laminated with spandex fabric commonly seen on diving suits and sports apparel accessories. Known for the comfort it provides, this material protects the individual using the brace from the discomfort caused by the ridges of the hinged structure when in its corrugated form. A padded Neoprene ankle/wrist strap (Pingmall ankle strap) covers the wrist protecting it from discomfort and also fixing the hinged laminate to the wrist joint. Additional cushioning is provided on the forearm section of the glove to protect the user’s skin from the high loads generated on this area when the user tries to bend his/her arm downwards with the rigid mode of the device activated.

## MODELING

### Three Point Bending

To understand the relationship between geometrical parameters and the hinged structure’s bending stiffness, we developed an

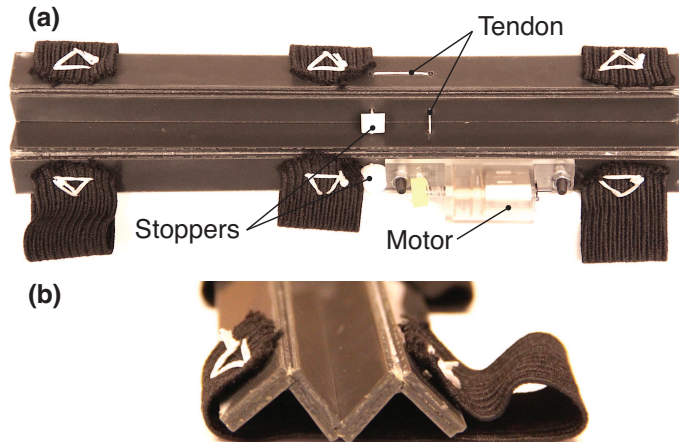


**FIGURE 3:** The tendon driven system. (a) Corrugated shape. (b) Side view.

analytical model, using the three-point bending test as a generic measure of rigidity [20, 21].

$$k = \frac{48EI}{L_{\text{eff}}^3} \quad (1)$$

where  $E_b$  is the bending modulus,  $I$  is the second moment of area and  $L_{\text{eff}}$  is the effective length (distance between supports).

The laminate hinged structure consisted of  $n$  laminate sections, each with two plates on either side of the flexural layer, connected by flexural hinges as seen in Fig. 2. Because the plates have two different widths to accommodate folding, this arrangement includes  $n+1$  beams with larger width  $w_1$  and  $n-1$  beams with smaller width  $w_2$ . Thickness  $t$ , bending modulus  $E$  and effective length  $L_{\text{eff}}$  are the same for both flat and corrugated modes. Therefore, the stiffness ratio is ultimately given by the ratio of the second moment of areas in the corrugated and flat shape respectively as given by Eqn.2.

$$\frac{k_c}{k_f} = \frac{I_c}{I_f} \quad (2)$$

where  $I_f$  and  $I_c$  correspond to the second moment of area of the structure in its flat and corrugated positions, respectively. For the hinged structure presented here, Eqn.3 and Eqn.4 can be used to calculate this geometrical property for both operational modes (flat and corrugated), respectively.

$$I_f = \frac{t^3 w_1 (n+1)}{12} + \frac{t^3 w_2 (n-1)}{12} \quad (3)$$

$$I_c = (n+1) \left( \frac{tw_1^3}{24} - \frac{\cos(2\theta) \left( \frac{tw_1^3}{12} - \frac{t^3 w_1}{12} \right)}{2} + \frac{t^3 w_1}{24} \right) + (n-1) \left( \frac{tw_2^3}{24} - \frac{\cos(2\theta) \left( \frac{tw_2^3}{12} - \frac{t^3 w_2}{12} \right)}{2} + \frac{t^3 w_2}{24} \right) \quad (4)$$

These equations indicate that we can tune the stiffness of the structure by changing the corrugation angle  $\theta$ .

## EXPERIMENTS AND RESULTS

In order to characterize the wrist brace, we ran tests designed for bending modulus, model validation, material selection, and

performance under simulated conditions for a hinged structure implemented on a wrist brace. Each test was performed on three samples with a Mecmesin Multi-Test 2.5i coupled with a 250 N or 2500 N load cell depending on the test. Referring to Fig. 2, samples were made with a larger width  $w_1$  of 14 mm and smaller width  $w_2$  of 13 mm. For tests where applicable, corrugation angle  $\theta$  was kept at 45 degrees. In all bending tests, data of force as a function of displacement were obtained.

### Bending Modulus

Although the Young's modulus is sufficient to calculate bending stiffness in a three-point test, many polymers exhibit a different material stiffness under bending, known as the bending stiffness  $E_b$ . We performed a three point bending test to measure  $E_b$  for the following materials: nylon 6/6, polystyrene and nylon 645 (Lulzbot). Three samples of each material were tested with a maximum probe displacement of 10 mm. Each sample was a rectangular beam measuring 50.8 mm wide and 152 mm long. The effective length between supports was 102 mm.

Based on the force-displacement measurements and eqn.1, we calculated the bending modulus  $E_b$  for all three materials. The values obtained for nylon 6/6, polystyrene and nylon 645 were 3.29 GPa, 1.01 GPa and 1.06 Gpa respectively.

### Rigid Structure

We tested a monolithic corrugated structure in order to validate our model without having to account for flexural hinges. In this set of tests, we used a 3D Printer (LulzBot TAZ 6) to build three samples of rigid corrugated structures made with nylon 645

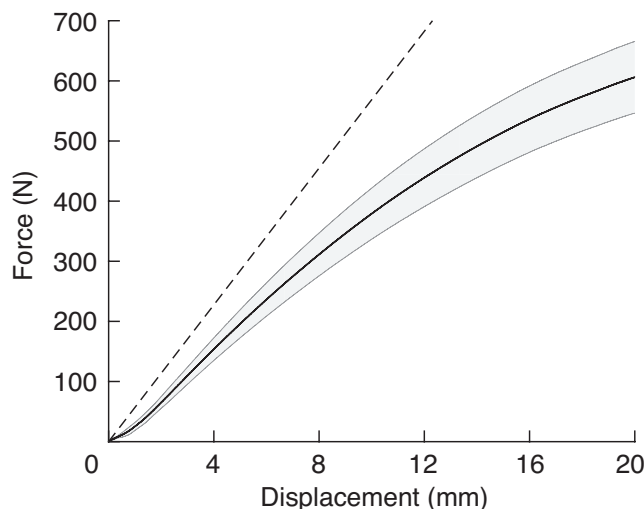


**FIGURE 4:** Model validation for a corrugated rigid beam structure made of nylon 645. Model (dashed line) and test results (solid with shaded region showing one standard deviation,  $N=3$ ).

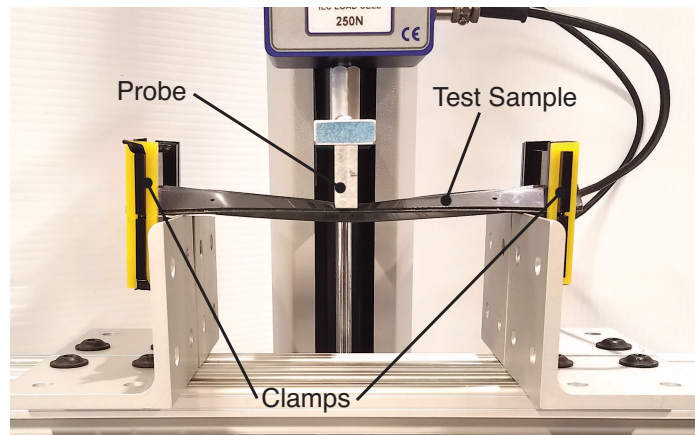


**FIGURE 5:** Three point bending test setup.

provided by the printer's manufacturer. The structure had a total length of 203 mm, an effective length between supports of 152 mm and was 3.2 mm thick. It included four corrugations, replicating the same overall shape as a hinged compliant structure with 16 beams. A total probe displacement of 20 mm was generated with a 2500 N load cell.

Results show that the model overestimated the structural stiffness (Fig. 4) by approximately 40%. We believe that this is primarily due to 3D printing techniques that allow for additional internal compliance between deposited material filaments, and secondarily to the limitations of an ideal bending model for an irregular cross-section, including a small nonlinear regime at the start of displacement.

### Hinged Structure

The intent of this set of tests was to observe the rigidity of the structure with flexural hinges and compare obtained results

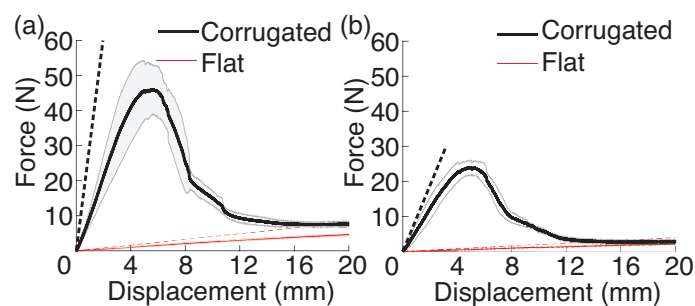


**FIGURE 6:** Varying materials test. a) Nylon 6/6 in corrugated (black) and flat (red) modes. b) Polystyrene in corrugated (black) and flat (red) modes. Shaded region indicates standard deviation,  $N=3$ . Dashed lines indicate model predictions for both corrugated and flat modes.

to the analytical model. We tested two different materials: nylon 6/6 and polystyrene. Corrugation during tests was provided by means of two light-weight clamps. Each sample consisted of a hinged structure with a total of eight individual beams. They also had a total length of 203 mm and was 1/32" (790  $\mu$ m) thick. We applied a three-point bending test with an effective length between supports of 152 mm (Fig. 5). A total probe displacement of 20 mm was generated with a 250 N load cell at 10 mm/min.

Nominal values for stiffness in the linear regime were measured for both corrugated and flat modes, and the ratio between them was calculated. As shown in Fig. 6, high stiffness ratios were observed during this set of tests. Nylon 6/6 demonstrated a ratio of 44.9 while polystyrene demonstrated a ratio of 57.2. However, we observed that polystyrene was more prone to delamination effects. Also, the maximum load of polystyrene was much smaller (peak in the corrugated shape at approximately 25 N) than the maximum load on nylon 6/6 (peak at approximately 55 N). These results both underperform compared to the 150-fold stiffness ratio predicted by the model. We expect that this is due to alternative deflection modes such as segment torsion and its effect on bending stiffness, as we observed these deflections during testing.

## INTEGRATED BRACE TESTING

In order to investigate the behavior of the laminate structure on a wrist brace, we performed another set of bending tests to simulate the wrist brace performance in its flat and corrugated form under wrist flexion. In this test, the wrist brace was mounted over an 80/20 frame with a rectangular cross-section of 50 mm wide by 31 mm thick. A constraining strap (Ping-

mall Ankle Strap) was tied around the simulated wrist area (end of the 80/20 frame) (Fig. 7) to fix the device to the wrist joint. Each of three samples consisted of a hinged structure made of nylon 6/6 with a total of 8 individual beams measuring 203 mm long and 1/16" thick (1.6 mm). Folding was actuated by a motor attached to one of the beams. Figure 8 shows the results compared to the maximum wrist torque and flexion of an average human as reported by Morse et al. [22] and supported by similar research [23–25].

The stiffness ratio obtained in the test between the corrugated and flat forms, determined by the slope between 0° and 10° was 4.1, substantially underperforming the model-predicted ratio of 38. In addition to the model limitations discussed in the three-point-bending results, we believe that the compliant attachment points between the structure and the wrist straps allowed for additional deflection (Fig. 7). We observed considerable displacement between the hinged structure and the simulated wrist region which limited the overall stiffness. Still, the stiffness ratio observed in this test demonstrated the concept of increased stiffness from a corrugated hinged structure. In the corrugated form, the average torque leveled off at about 3.9 N·m when deflection reached 30°, significantly below the maximum wrist torque of the average human maximum of 8 N·m. At this point, the variation between samples also increased substantially, as samples started to delaminate and buckle. In the flat state, the torque at maximum flexion was 3.4 N·m, below the maximum wrist torque but large enough to impede normal human movements. These

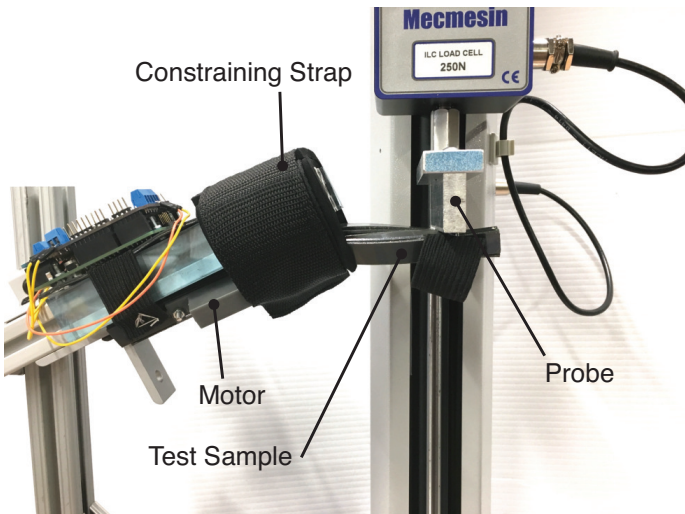


**FIGURE 7:** Experimental setup to simulate wrist flexion against the wrist brace with a cantilever test.

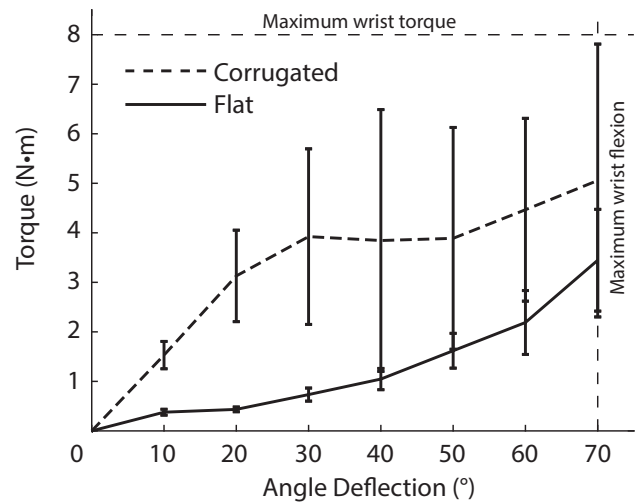


**FIGURE 8:** Torque exerted against the wrist brace as a function of angular deflection in both the flat (solid line) and corrugated (dashed line) states. The thin dashed lines represent the maximum wrist torque (8 N·m) and flexion (70°) of an average human [22]. Error bars indicate standard deviation, N=3

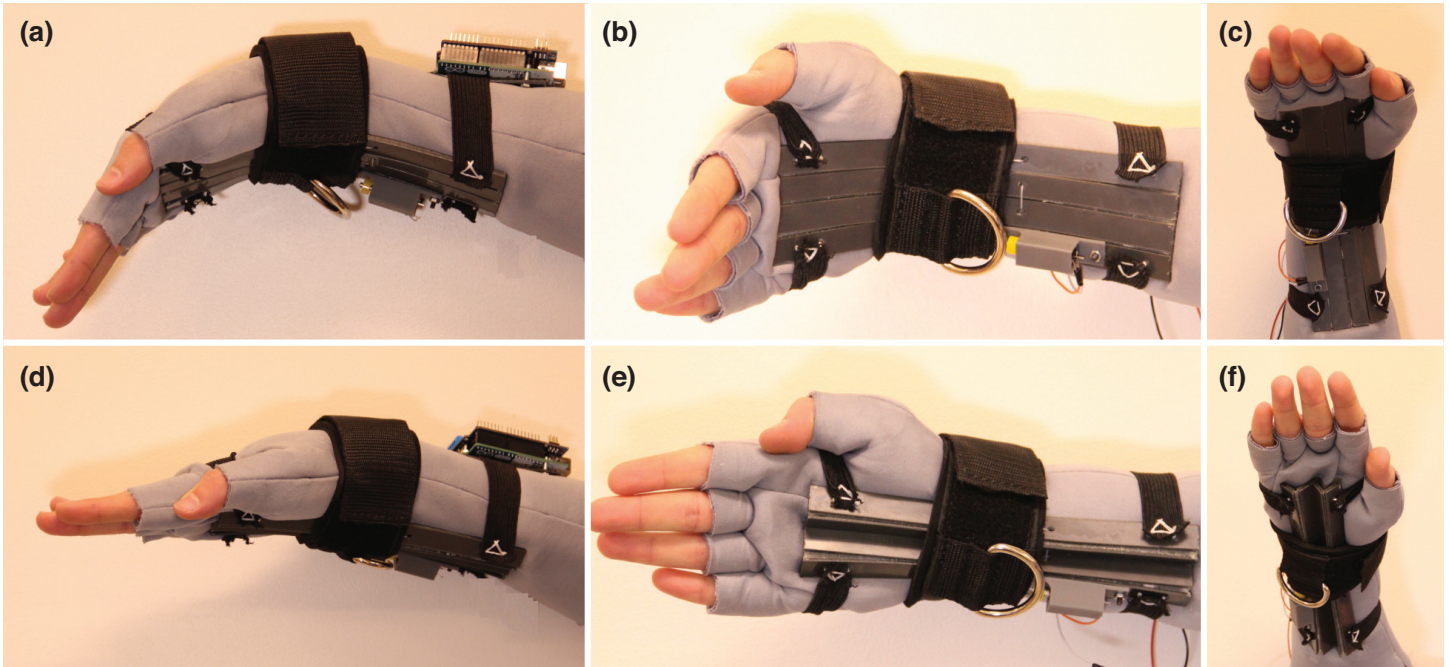


**FIGURE 9:** A wrist brace implementation. (a) Significant displacement during flat configuration. (b) Bottom view during flat configuration. (c) Side view during flat configuration. (d) Limited displacement during corrugated configuration. (e) Bottom view during corrugated configuration. (f) Side view during corrugated configuration.

results indicate that further work must be done to optimize the brace to fully resist wrist torque in the corrugated state while remaining flexible in the flat state.

We demonstrated the full device on a human (Fig. 9). When the wrist brace is flat, we can achieve substantial deflection (Fig. 9a-c). When the wrist is in corrugated configuration, wrist movement is constrained (Fig. 9d-f).

## CONCLUSION

This research indicates that an origami approach to variable stiffness structures can be implemented in orthopedic devices. The tendon based actuation method was efficient as no power was consumed once a state (either rigid or flexible) is reached. This is in contrast to pneumatic and temperature based methods that usually require intermittent power to maintain a flexible (or rigid) mode over long times. Also, its geometrical nature benefits applications where human safety and environmental issues establishes a limit for other approaches such as those associated with rheological fluids.

Three point bending tests showed that stiffness can be increased up to a factor of 44.9 using a corrugated design, a valuable property in dual-stiffness structures. However, it underperforms our model, and we expect that there are additional deflection modes that we must account for. In particular, we observed

torsion along the length of each segment, which not only allows for additional displacement, but reduces the bending stiffness of the beam by changing the corrugation angle  $\theta$ . Future efforts will take this behavior into account to more accurately predict bending stiffness of hinged structures. In addition, bending in only one direction is taken into account while in the tests it was noted that internal forces also induce a transverse bending of the beams with the ones further away from the longitudinal axis bending more than the central ones. Finally, it is noted that external loads are not uniformly distributed across the hinged laminate as the “ridges” constitute just a discrete amount of loaded points.

Once the mechanics of the structure are better understood, we plan to investigate other geometric mechanisms using a model-based approach. More complicated fold patterns such as a Miura-based pattern with orthogonal hinges could allow for much greater flexibility along the mechanism length. Non-folding approaches are also possible, including a sliding plate design where hinges are pushed into and out of alignment, locking them in place [15]. This would reduce the issues with a changing envelope, but introduce friction into the mechanism.

The design presented here was not tailored for ergonomics, but wearability and comfort are essential attributes of an orthopedic device. Therefore, we must further investigate ways to make the wrist brace comfortable and easily wearable without affecting performance. As observed during integrated brace tests, the cur-

rent method to obtain the necessary boundary conditions was still not satisfactory. We will design ergonomic attachment points for the palm, wrist, and forearm, taking previous inspiration from soft exoskeletons [26]. Given the large performance reduction between the isolated origami structure and its integration into the glove, we expect that these attachment points are critical to brace performance. Furthermore, the sharp edges of the folded structure apply uneven forces and can pinch or dig into the palm and forearm. This must be mitigated before it is tested on human subjects.

## REFERENCES

- [1] Sasaki, D., Noritsugu, T., and Takaiwa, M., 2005. “Development of active support splint driven by pneumatic soft actuator (assist)”. In *Robotics and Automation, 2005. ICRA 2005. Proceedings of the 2005 IEEE International Conference on*, IEEE, pp. 520–525.
- [2] Letts, R., and Hobson, D., 1973. “The vacuum splint: an aid in emergency splinting of fractures”. *Canadian Medical Association Journal*, **109**(7), p. 599.
- [3] Ding, Y., Galiana, I., Asbeck, A., Quinlivan, B., De Rossi, S. M. M., and Walsh, C., 2014. “Multi-joint actuation platform for lower extremity soft exosuits”. In *Robotics and automation (ICRA), 2014 IEEE international conference on*, Ieee, pp. 1327–1334.
- [4] Coppard, B. M., and Lohman, H., 2008. *Introduction to splinting*. Elsevier Health Sciences.
- [5] Blanc, L., Delchambre, A., and Lambert, P., 2017. “Flexible medical devices: Review of controllable stiffness solutions”. *Actuators*, **6**(3), p. 23.
- [6] Jafari, A., Tsagarakis, N. G., and Caldwell, D. G., 2013. “A novel intrinsically energy efficient actuator with adjustable stiffness (awas)”. *IEEE/ASME transactions on mechatronics*, **18**(1), pp. 355–365.
- [7] Cheng, N. G., Gopinath, A., Wang, L., Iagnemma, K., and Hosoi, A. E., 2014. “Thermally tunable, self-healing composites for soft robotic applications”. *Macromolecular Materials and Engineering*, **299**(11), pp. 1279–1284.
- [8] Loeve, A. J., Bosma, J. H., Breedveld, P., Dodou, D., and Dankelman, J., 2010. “Polymer rigidity control for endoscopic shaft-guide ‘plastolock’—a feasibility study”. *Journal of Medical Devices*, **4**(4), p. 045001.
- [9] Carlson, J. D., Matthis, W., and Toscano, J. R., 2001. “Smart prosthetics based on magnetorheological fluids”. In *Smart Structures and Materials 2001: Industrial and Commercial Applications of Smart Structures Technologies*, Vol. 4332, International Society for Optics and Photonics, pp. 308–317.
- [10] Manti, M., Cacucciolo, V., and Cianchetti, M., 2016. “Stiffening in soft robotics: A review of the state of the art”. *IEEE Robotics & Automation Magazine*, **23**(3), pp. 93–106.
- [11] Kim, Y.-J., Cheng, S., Kim, S., and Iagnemma, K., 2012. “Design of a tubular snake-like manipulator with stiffening capability by layer jamming”. In *Intelligent Robots and Systems (IROS), 2012 IEEE/RSJ International Conference on*, IEEE, pp. 4251–4256.
- [12] Kim, Y.-J., Cheng, S., Kim, S., and Iagnemma, K., 2013. “A novel layer jamming mechanism with tunable stiffness capability for minimally invasive surgery”. *IEEE Transactions on Robotics*, **29**(4), pp. 1031–1042.
- [13] Bureau, M., Keller, T., Perry, J., Velik, R., and Veneman, J. F., 2011. “Variable stiffness structure for limb attachment”. In *Rehabilitation Robotics (ICORR), 2011 IEEE International Conference on*, IEEE, pp. 1–4.
- [14] Kim, S.-J., Lee, D.-Y., Jung, G.-P., and Cho, K.-J., 2018. “An origami-inspired, self-locking robotic arm that can be folded flat”. *Science Robotics*, **3**(16), p. eaar2915.
- [15] Park, Y.-J., Lee, J.-G., Jeon, S., Ahn, H., Koh, J., Ryu, J., Cho, M., and Cho, K.-J., 2016. “Dual-stiffness structures with reconfiguring mechanism: Design and investigation”. *Journal of Intelligent Material Systems and Structures*, **27**(8), pp. 995–1010.
- [16] Liu, C., and Felton, S. M., 2017. “A self-folding robot arm for load-bearing operations”. In *Intelligent Robots and Systems (IROS), 2017 IEEE/RSJ International Conference on*, IEEE, pp. 1979–1986.
- [17] Katz, J. N., and Simmons, B. P., 2002. “Carpal tunnel syndrome”. *New England Journal of Medicine*, **346**(23), pp. 1807–1812.
- [18] Tolley, M. T., Felton, S. M., Miyashita, S., Aukes, D., Rus, D., and Wood, R. J., 2014. “Self-folding origami: shape memory composites activated by uniform heating”. *Smart Materials and Structures*, **23**(9), p. 094006.
- [19] Wood, R. J., Avadhanula, S., Sahai, R., Steltz, E., and Fearing, R. S., 2008. “Microrobot design using fiber reinforced composites”. *Journal of Mechanical Design*, **130**(5), p. 052304.
- [20] Hibbeler, R. C., 2013. *Statics and mechanics of materials*. Pearson Higher Ed.
- [21] Boresi, A. P., Schmidt, R. J., and Sidebottom, O. M., 1993. *Advanced mechanics of materials*, Vol. 6. Wiley New York.
- [22] Morse, J. L., Jung, M.-C., Bashford, G. R., and Hallbeck, M. S., 2006. “Maximal dynamic grip force and wrist torque: The effects of gender, exertion direction, angular velocity, and wrist angle”. *Applied Ergonomics*, **37**(6), pp. 737–742.
- [23] Vanswearingen, J. M., 1983. “Measuring wrist muscle strength”. *Journal of Orthopaedic & Sports Physical Therapy*, **4**(4), pp. 217–228.
- [24] Arner, M., and Hagberg, L., 1984. “Wrist flexion strength after excision of the pisiform bone”. *Scandinavian journal*

- of plastic and reconstructive surgery*, **18**(2), pp. 241–245.
- [25] Salonikidis, K., Amiridis, I. G., Oxyzoglou, N., de Vil-lareal, E. S. S., Zafeiridis, A., and Kellis, E., 2009. “Force variability during isometric wrist flexion in highly skilled and sedentary individuals”. *European journal of applied physiology*, **107**(6), pp. 715–722.
- [26] Asbeck, A. T., De Rossi, S. M., Holt, K. G., and Walsh, C. J., 2015. “A biologically inspired soft exosuit for walking assistance”. *The International Journal of Robotics Research*, **34**(6), pp. 744–762.